12B.1 DIFFERENCE OF RAINFALL DISTRIBUTION FOR TROPICAL CYCLONES OVER LAND AND OCEAN AND RAINFALL POTENTIAL DERIVED FROM SATELLITE OBSERVATIONS AND ITS IMPLICATION ON HURRICANE LANDFALL FLOODING PREDICTION

Haiyan Jiang[1]*, Jeffrey B. Halverson[1], and Joanne Simpson[2]
[1]Joint Center for Earth Systems Technology, University of Maryland Baltimore County, Baltimore, MD, and Mesoscale Atmospheric Process Branch, NASA Goddard Space Flight Center, Greenbelt, MD
[2]Laboratory for Atmospheres, NASA Goddard Space Flight Center, Greenbelt, MD

1. INTRODUCTION

Predicting hurricane landfall precipitation is a major operational challenge. Inland flooding has become the predominant cause of deaths associated with hurricanes in the United States (Rappaport 2000). The tropical cyclone (TC) track forecast has been improved in accuracy of 20% over a 5-yr period, which is the achievement of the first research goal of the U.S. Weather Research Program (USWRP) Hurricane Landfall (HL) focus (Elsberry 2005). However, the difficulties of improving 72-h quantitative precipitation forecast for TCs, thereby improving day 3 forecasts for inland flooding, have been long recognized. TC rains are multi-scale in nature. Mesoscale convective system could contribute crucial amount of TC rain, but its space and time variation is hard to predict (Heymsfield et al. 2001). Once a storm makes landfall, additional factors such as the presence of significant topography and extratropical transition come into play (Carr and Bosart 1978, Atallah and Bosart 2003).

Early precipitation studies of TCs over land have been confined to rain gauge data. Miller (1958) examined the composite and frequency distribution of hourly rain amounts for 16 Florida hurricanes with respect to their center. He found that the mean rain rate in the 1° box directly surrounding the storm center was about a factor of 2 higher than the mean rain rate in the remaining outer domain. Significant asymmetric characteristics of the hurricane rainfall over land were also recognized.

Satellites provide the most common means for monitoring TC rainfall for both over ocean and land. Satellite-based statistical analysis of TC rainfall characteristics is critical to understand and improve quantitative precipitation forecast in TCs. Rogders and Alder (1981) constructed radial profiles of rainfall for a set of North Pacific TCs using data from the Nimbus-5 Electrically Scanning Microwave Radiometer (ESMR-5). The sample included 71 ESMR-5 observations of 21 western and eastern North Pacific Ocean TCs at different stages of development during 1973, 1974, and 1975. There were 49 observations of 18 western Pacific TCs and 22 observations of 3 eastern Pacific TCs.

These observations were mainly over ocean. Rogders and Alder (1981) found that the maximum azimuthally average rain rate is about 5 mm h^{-1} for typhoons, but decreases to 3.5 mm h^{-1} for tropical storms, to 3 mm h^{-1} for depressions, and to 1.5 mm h^{-1} for disturbances. They also found that TC intensification was accompanied not only by increases in the average rain rate, but also in the relative contribution of the heavy rainfall.

Rao and MacArthur (1994) examined 12 western North Pacific typhoons of mainly the 1987 season and the associated precipitation fields derived from Special Sensor Microwave/Imager (SSM/I) brightness temperatures. Of the 27 observations, only 4 observations contained over land pixels. Majority of the sample were over ocean. They found that the mean rainfall rate within 0.5° box is 2.6 mm h^{-1}, decreases to 2.5 mm h^{-1} within 0.5°-1° annulus, to 2.0 mm h^{-1} within 1°-2° annulus, and to 1.5 mm h^{-1} within 2°-3° annulus, and to 1.2 mm h^{-1} within 3°-4° annulus. Their study also showed that rainfall rates were highly correlated with 24-h future typhoon intensity.

With dramatically larger sample size, Rodgers and Pierce (1995) examined precipitation characteristics derived from SSM/I observations for western North Pacific tropical depressions, tropical storms, and typhoons occurring during the period from 1987 through 1992. The radial distribution of rainfall rate was constructed from 1018 over ocean observations of 162 TCs. They found that the maximum azimuthally average rain rate is about 8.5 mm h^{-1} for strong typhoons, but decreases to 5.5 mm h^{-1} for weak typhoons, to 4.8 mm h^{-1} for tropical storms, and to 2.8 mm h^{-1} for depressions. Rodgers et al. (1994) performed a similar study using western North Atlantic TCs, but with a much smaller sample size. A total of 108 observations of 18 named TCs that traversed the land-free western North Atlantic ocean during 1987-1989 were used. They found that the maximum azimuthally average rain rate is about 6.4 mm h^{-1} for hurricanes, but decreases to 4.8 mm h^{-1} for tropical storms, and to 3.8 mm h^{-1} for depressions.

Using 2121 Tropical Rainfall Measurement Mission (TRMM) microwave imager observations of 260 TCs over the global oceans during 1998-2000, Lonfat et al. (2004) showed that the maximum azimuthally averaged rainfall rate is about 12 mm h^{-1} for category 3-5 hurricane-strength systems, but decreases to 7 mm h^{-1} for category 1-2 storms, and to 3 mm h^{-1} for tropical

* *Corresponding author address*: Haiyan Jiang, NASA GSFC, Code 613.1, Bldg 33, Rm C415, Greenbelt, MD 20771; e-mail: Jiang@agnes.gsfc.nasa.gov

storms. No over-ocean and over-land conditions were separated.

When the storm is over ocean, its rain is well correlated with storm maximum wind intensity; while over land, this kind of relationship might be much weaker due to additional factors. Therefore, the first goal of the present study is to determine the differences of TC rainfall distributions for over ocean and over land conditions.

Hurricanes or typhoons, even tropical storms, can produce torrential rains during landfall, especially if they are the remnants of a much stronger circulation. Floods by TCs are associated not only the storm's maximum wind intensity, but also its history, its projected movement, and its size. Regardless of the complicated factors including topography and trough interactions that influence the hurricane landfall and inland rainfall, Malkus and Riehl (1960) found that the cloud/rain pattern of many storms was quite similar from day to day. In addition, Griffith et al. (1978) noted great variability in storm total rainfall from system to system. Griffith et al. (1978) further proposed a hypothesis that knowing the rainfall history or “wetness” of a storm as it evolves over ocean, one may use this information to predict the storm’s potential for catastrophic inland flooding. They defined a parameter called rainfall potential, which is defined by using an estimated average rain rate derived from infrared (IR) satellite observations, combined with the storm size and translation speed information. The rainfall potential histories of a dozen TCs approaching landfall were examined. Their method correctly predicted the highest actual rainfall totals for the major flood hurricanes Agnes (1972) and Fifi (1974), and the lowest potentials for relatively dry hurricanes Celia (1970) and Edith (1971).

With the advantages of better physical connection between microwave observations and precipitation and high spatial and temporal resolution of IR observations, a combined microwave-IR rainfall product can provide better precipitation estimates globally than any microwave only or IR only products (Adler et al. 1993, 1994, 2003; Huffman et al. 2001). In the framework of the TRMM project, the National Aeronautic and Space Administration (NASA) Multi-satellite Precipitation Analysis (MPA) has produced gridded 3-h precipitation rate estimates with relatively high horizontal resolution (0.25° x 0.25° longitude/latitude) since January 1998. These rainfall estimates are based on microwave information provided by various low-orbiting satellites, merged with IR-based estimates from geostationary meteorological satellites (Huffman et al. 2002). TRMM products are used to calibrate the estimates. Applying the new MPA rainfall estimates to Griffith et al. (1978)’s technique, Jiang et al. (2005) examined the difference of rainfall potential history of hurricane Isidore and Lili (2002). Isidore produced much heavier rain as a greatly weakened tropical storm than category 1 hurricane Lili during landfall over the same area. Jiang et al. (2005) showed that the average rainfall potential during 4 days before landfall for Isidore was over a factor of 2.5 higher than that for Lili. The second goal of present study is to examine the relationships between the rain potential before landfall and storm rainfall parameters during landfall for 37 TCs over the Atlantic during 1998-2004 by using the MPA product.

Section 2 presents a description of MPA data, the definition of rain potential, method used to analyze the MPA rainfall parameters and case studies, and hurricane best track and landfall rain information. Section 3 uses the MPA rainfall product to determine the rainfall distribution of North Atlantic TCs during 1998-2004 over ocean and land. Section 4 presents the relationships between rain potential before landfall and storm rainfall parameters during landfall and introduces an index for TC landfall rain forecast. Section 5 summaries the work.

2. DATA AND METHODS

a. MPA product

The NASA Goddard Multi-satellite Precipitation Analysis (MPA) product used in this study is provided by two different sets of sensors. Microwave data are collected by various low-orbit satellites, including TRMM Microwave Imager (TMI), the Special Sensor Microwave/Imager (SSM/I), the Advanced Microwave Scanning Radiometer for the Earth Observing System (AMSR-E), and the Advanced Microwave Sounding Unit (AMSU). Precipitation estimates are made from TMI, SSM/I, and AMSR-E microwave data by applying the Goddard Profiling Algorithm (GPROF, Kummerow et al., 1996). AMSU microwave measurements are converted to rainfall estimates by using the AMSU-B algorithm (Zhao and Weng 2002; Weng et al. 2003). High Quality (HQ) microwave estimates are produced by using the TRMM Combined Instrument (TCI) to calibrated microwave precipitation estimates. The TCI utilizes the superior horizontal resolution of the TMI and TRMM Precipitation Radar (PR) to produce a high quality merged microwave rainfall estimate. IR data are collected by the international constellation of Geosynchronous-Earth-Orbit (GEO) satellites. IR estimates are calibrated with the HQ microwave estimates. The microwave and GEO-IR estimates are merged in a probability-matched method (Huffman et al., 2003). A post-real-time product called MPA (in the framework of TRMM, it is also referred as TRMM 3B42) is produced from the merged microwave-IR dataset. The MPA dataset consists of gridded precipitation rate files with 0.25° x 0.25° longitude/latitude horizontal resolution, within the global latitude belt 50°S to 50°N. The temporal resolution is 3 hours and the files are generated on synoptic observations times (00 UTC, 03 UTC, ..., 21 UTC). In this study, the TRMM version 6 of MPA product is used.

b. Tropical Cyclone Best Track and Landfall Rain Information

North Atlantic TC post-analysis best tracks for 1998-2004 were provided by the National Hurricane Center (NHC, now known as the Tropical Prediction Center). Dr. Mark DeMaria at Colorado State University created the extended best track dataset for 1988-2004 (ftp://ftp.cira.colostate.edu/demaria/ebtrk) to include storm size information that was not in the standard NHC best track data. The post-analysis merges available data to produce a (sometime smoothed) time history of the cyclone's center position, maximum sustained winds, and minimum sea level pressure for every 6 h. The available data sources include ship and other surface reports, aircraft reconnaissance data and satellite imagery. At present, there are no error estimates for these variables. Generally speaking, these parameters are more reliable west of 55 longitude, where aircraft reconnaissance data is usually available.

According to the best track information, a dataset including 37 North Atlantic TCs that made landfall in the U.S. Gulf during 1998-2004 is set up. For each landfall TC, its maximum storm total rain during landfall is provided by the Tropical Cyclone Rainfall Data webpage (http://www.hpc.ncep.noaa.gov/tropical/rain/tcrainfall.html) built by Dr. David Roth at National Oceanic and Atmospheric Administration (NOAA) Hydrometeorological Prediction Center (HPC). This TC overland rainfall database is based on rain gauge observations from the National Climate Data Center, National Weather Service River Forecast Centers, many local Water Management and Networks, and additional NHC reports (David Roth, personal communication 2005). The maximum storm total rain represents the maximum value of the storm accumulated rains during the storm's US land-rain period (the days when the storm rains over the US land) for all rain gauge stations. Table 1 lists the 37 landfall TCs, their maximum surface wind, intensity stage during landfall in the US Gulf coast, US landfall date (when the storm center is over land), US land-rain period, and maximum storm total rains during US landfall period. Table 1 also lists the mean daily rain over land, mean daily volumetric rain over land, and storm total volumetric rain on the landfall day. These 3 parameters are derived from the MPA product.

c. Definition of Rain Potential

This study adapts the hypothesis proposed by Griffith et al. (1978) to assess the flooding potential of approaching TCs using a parameter called mean total rain potential, defined as:

$$\text{mean total rain potential}=\frac{\overline{D}\overline{d}}{\overline{v}}, \qquad (1)$$

where $\overline{D}$ is MPA daily average storm rainfall (mm day^{-1}), $\overline{d}$ the mean cross section (km) of the storm as measured from the satellite image in the direction of motion, and $\overline{v}$ the mean storm translation speed (km day^{-1}) derived from hurricane best-track data. The mean cross section $\overline{d}$ is obtained manually by measuring the MPA daily rain accumulation images.

d. Analysis Method

To determine the rainfall characteristics of TC for over ocean and land, a total of 2680 3- hourly MPA bservations for the whole life time of the 37 TCs are separated for over-ocean and over-land categories. The criterion is if one observation contains 80% of pixels over ocean (land), then this observation is attributed to over-ocean (over-land) category. For observations that are not identified either over-land or over-ocean, we call those as "Between". The data is also categorized by the storm intensity stage: tropical depressions (TDs) are defined as system with wind speed less than 17 m s^{-1}, tropical storms (TSs) as systems with wind between 18 to 33 m s^{-1}, and hurricanes (HURs) as systems with wind>34 m s^{-1}. Table 2 shows the numbers of the MPA observations for each category. The MPA rainfall parameters are derived in storm-relative coordinates. The azimuthally mean values are calculated in 28-km-wide annuli around the storm center outward to the 1111-km radius for MPA-derived parameters. The resulting dataset allows us to examine the radial dependence of parameters as a function of time. The conditional (only when raining) probability density functions (PDFs) of rain rate with radial distance can also been determined using the annular dataset. Using the annular PDFs, a contoured frequency by radial distance (2-D frequency) diagram can be constructed as a function of storm intensity and location (e.g., over ocean or land).

The next step of our study consists in computing the linear correlations between the daily rainfall potential derived when the storm is over ocean and storm's landfall precipitation parameters. One of these parameters is the maximum storm total rain during landfall obtained from rain gauge observations (section 2b), the other is the storm total volumetric rain during landfall. The storm total volumetric MPA rain is calculated within the cyclone region. The storm size as a function of time is determined according to MPA images. Then inside the storm, total volumetric parameters ($\sum X$) can be expressed as:

$$\sum X = \sum_{i=0}^{i=n} X_i A \qquad (2)$$

where X represents MPA rain rate, A is the area of each single pixel. For MPA rain rate, A is 0.25°x 0.25°. n is the number of data points inside the storm.

3. DISTRIBUTION OF TC RAINFALL OVER LAND AND OCEAN

a. PDF of Rain Rates

Fig. 1 shows the PDF distributions of rain rates for all MPA rainfall observations within an area of 1111-km (10° radius) around the storm center. The mode is near 1 mm hr^{-1}, but not unique, as the over-ocean PDF has a mode of 1 mm hr^{-1}, while the over-land PDF shows a mode of about 1.2 mm hr^{-1} (Fig. 1b). Not only the mode of the over-land distribution is higher than that for the over ocean distribution, but also the over-land distribution tends to be broader than the over-ocean distribution. For the TC intensity groups (Fig. 1c), as the storm intensity increases, the mode of the distribution shift toward higher values and the distribution tends to become broader. This is as same as what was found by Lonfat et al. (2004).

Similar characteristics can be seen in the different intensity PDFs for over-land (Fig. 1d) and over-ocean (Fig. 1e) groups. The land/TD distribution is similar to the overall over-land PDF, which is not surprising as more percentage of over-land observations is in depression stage due to the land interaction effect on decreasing the storm intensity. Both land/TS and land/HUR PDFs have higher modes and broader distributions than those overall TS and HUR PDFs (Fig. 1c). Even a second maximum of about 4 mm hr^{-1} can be seen in the over-land hurricane distribution, which indicates that hurricane rain during landfall tends to be stronger than over ocean. All the over-ocean TD, TS, and HUR distributions (Fig. 1e) are similar to the overall TD, TS, HUR PDFs (Fig. 1c), which is because more over-ocean observations were observed.

Table 1: Landfall rain parameters derived from MPA product (the last 3 columns) and from surface rain gauge observations (7th column) for 37 North Atlantic Tropical cyclones during 1998-2004.

Year	Name	Max. Wind (kt)	Land-fall Stage	US Landfall Date (mmdd hhmm)	Land-rain Period in US (mm/dd-mm/dd)	Max. Storm Total Rain During Landfall in US (mm)	Mean Daily Rain Over Land (mm day^{-1})	Mean Daily Volume-tric Rain Over Land (km^3 day^{-1})	Storm Volume-tric Rain On Landfall Day (km^3 day^{-1})
1998	Bonnie	100	TS	08270400	08/26-08/29	371.09	4.45	9.76	22.58
1998	Charley	60	TS	08221000	08/20-08/25	483.87	18.33	6.05	12.32
1998	Earl	85	Hur	09030600	09/01-09/06	415.54	14.30	30.62	42.71
1998	Frances	55	TS	09110600	09/07-09/17	568.71	12.65	37.61	59.83
1998	Georges	135	Hur	09251530	09/24-10/01	976.88	52.97	12.31	35.10
1998	Hermine	40	TS	09200500	09/17-09/22	359.16	3.56	7.43	11.52
1998	Mitch	155	TS	11051100	11/04-11/05	284.48	6.32	16.07	91.77
1999	Bret	125	Hur	08230000	08/22-0825	334.77	8.90	5.58	7.41
1999	Dennis	90	Hur	09042100	08/24-09/06	350.52	2.71	5.28	17.50
1999	Floyd	135	Hur	09160630	09/14-09/17	611.12	68.47	37.20	48.71
1999	Harvey	50	TS	09211700	09/19-09/22	254.00	6.33	11.21	30.13
1999	Irene	95	Hur	10151300	10/12-10/17	443.23	16.17	25.42	85.86
2000	Gordon	70	TS	09180300	09/14-09/21	240.79	3.56	6.90	16.17
2000	Helene	60	TS	09221200	09/19-09/24	243.84	8.07	21.23	35.19
2001	Allison	50	TS	06052100	06/04-0617	1033.27	5.22	5.26	36.13
2001	Barry	60	TS	08060500	08/01-08/08	297.18	2.63	8.71	17.42
2001	Gabrielle	70	TS	09141200	09/10-09/16	383.54	6.79	12.61	46.61
2002	Bertha	35	TS	08090800	08/03-08/09	260.35	2.28	1.17	1.89
2002	Edouard	55	TS	09050045	09/02-09/07	194.06	4.14	2.86	5.91
2002	Fay	50	TS	09070900	09/05-09/11	469.65	5.74	13.81	22.42
2002	Gustav	85	TS	09120900	09/08-09/12	152.40	9.03	6.06	14.26
2002	Hanna	50	TS	09141500	09/12-09/15	395.22	7.26	16.61	29.98
2002	Isidore	110	TS	09260600	09/20-09/29	469.90	12.93	63.09	76.68
2002	Kyle	75	TS	10112200	10/09-10/12	221.49	13.38	32.23	44.46
2002	Lili	125	Hur	10031300	10/02-10/05	213.36	9.73	15.22	25.25
2003	Bill	50	TS	06301900	06/27-07/03	259.08	8.29	20.35	37.87
2003	Claudette	75	Hur	07151530	07/14-07/18	168.15	3.79	3.19	9.88
2003	Grace	35	TS	08311100	08/30-09/04	263.14	6.30	24.68	38.13
2003	Henri	50	TS	09060900	09/02-09/17	230.89	7.29	9.89	24.06
2003	Isabel	145	Hur	09181700	09/17-09/21	513.08	18.43	13.97	32.97
2004	Bonnie	55	TS	08121400	08/11-08/14	154.18	13.62	21.90	35.71
2004	Charley	125	Hur	08141600	08/12-08/15	250.95	7.93	12.14	21.55
2004	Frances	125	Hur	09050430	09/03-09/11	598.68	39.93	6.58	25.05
2004	Gaston	65	TS	08291400	08/25-09/01	320.04	7.87	5.23	9.77
2004	Ivan	145	Hur	09160650	09/13-09/26	431.80	15.95	39.20	47.08
2004	Jeanne	105	Hur	09260400	09/25-09/30	304.04	7.24	8.96	20.35
2004	Matthew	40	TS	10101100	10/06-10/15	457.20	7.58	23.66	46.87

Table 2: The number of MPA observations for each category.

	TD	TS	HUR	Total
Over Ocean	482	790	713	1985
Over Land	284	117	20	421
Between	116	105	53	274
Total	882	1012	786	2680

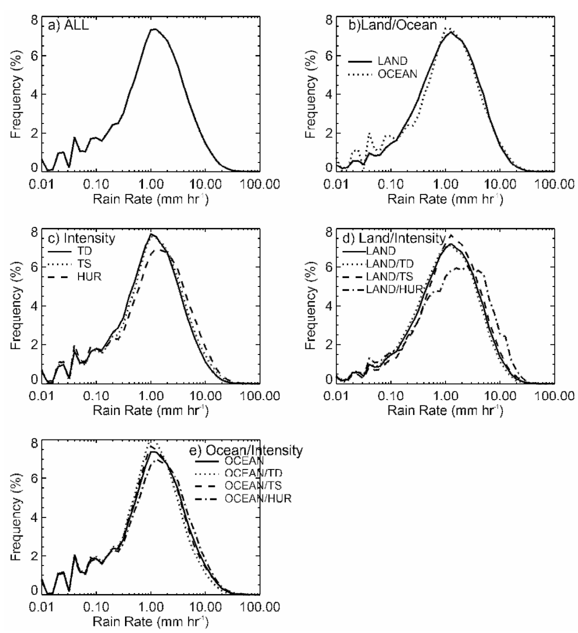

Figure 1. Probability density functions calculated within 10° radius of storm center a) for all 2680 observations, b) for over-land and over-ocean groups, c) for TC intensity groups, d) for over-land intensity subgroups, and e) for over-ocean intensity subgroups.

b. Azimuthal Averages

The radial distributions of azimuthally averaged rain rates for each of the three storm intensity categories in the over-land and over-ocean observations are shown in Fig. 2. The maximum azimuthally mean rain rate for all over-land observations is about 1.6 mm hr^{-1} within 50 km of the TC center (Fig. 1a), while the maximum azimuthally mean rain rate for all over-ocean observations is about 5.0 mm hr^{-1} within 50 km of the TC center (Fig. 1a). All over-land (over-ocean) mean rain rate decreases to 1 mm hr^{-1} at about 200 km (250 km), while both of over-land and over-ocean rain rates decreases to 0.5 mm hr^{-1} at about 400 km. Mean rain rates increase with storm intensity at all radii for both over-land and over-ocean observations. Peak mean rates are 1.0, 2.2, 9.5 (1.8, 2.5, 8.0) mm hr^{-1} for TD, TS, and HUR systems of over-land (over-ocean) observations, respectively. The location of the peak rainfall also varies with intensity, from about 70 (70) km from the storm center for TD to 15 (40) km for HUR for over-land (over-ocean) groups.

Previous studies (Rogders and Alder 1981, Rao and MacArthur 1994, Rodger et al. 1994, Rodger and Pierce 1995, Lonfat et al. 2004) on the radial distributions of azimuthally averaged rainfall rates of TCs showed the similar characteristics as Fig. 2b for over-ocean observations, expect that the values of rain rate estimates had some difference due to using different kind of observation means or retrieval strategies, but the magnitude of these estimates showed no significant discrepancy. However, for over-land distributions showed in Fig. 2a, significant difference with over-ocean (or overall in case of Lonfat et al. 2004) distribution can be identified, especially for the HUR category. It is obvious that correlations between rain rates and storm intensity still hold for over-land observations, but would be weaker than that for over-ocean observations. For the HUR category, the peak rain rate for over-land observations is higher and the location of this peak is much closer to the storm center than those for over-ocean observations.

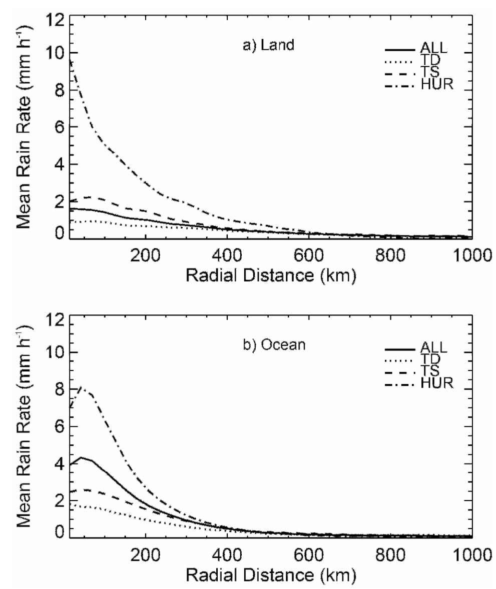

Figure 2. Mean rain rates as a function of radial distance for different TC intensity for a) over-land and b) over-ocean categories.

c. Rain Rate Distribution with Radial Distance

Fig. 3 and 4 show the rain rate 2D frequency distributions with radial distance to the storm center. The 2D frequencies are computed outward to the 1111-km radius from the TC center. Fig. 3 shows the 2D frequencies for all, over-land, and over-ocean observations. From Fig. 3a, the mode of the overall 2D frequency decreases from 4 mm hr^{-1} in the inner 50 km to 1 mm hr^{-1} by the 400-km radius. At ranges > 400 km, the peak remains at 1 mm hr^{-1}. The over-ocean 2D frequency (Fig. 3c) is very similar to the overall distribution showed in Fig. 3a. Again, this is because the majority of the observations were observed over ocean. The over-land distribution showed in Fig. 3b is “flat”, the mode keeps at about 1 – 1.5 mm hr^{-1} for all radii. Over-land observations have a broader distribution than overall and over-ocean observations in the inner 200 km. Assuming that the width of the distribution is a measure of the asymmetric nature of the TCs (Lonfat et al. 2004), TCs over land seem more asymmetric in the inner core. In the region beyond 200 km, the 2D frequency of overall and over-ocean TCs broaden, indicating an increase in the asymmetry amplitude.

Fig. 4 presents the 2D frequency distributions grouped by storm intensity for over-land and over-ocean observations. The distributions vary with storm intensity. The mode of the land/TD distribution (Fig. 4a) is around 1 mm hr^{-1} for all radii, while the mode of the ocean/TD distribution (Fig. 4b) decreases from 2 mm hr^{-1} in the inner 100 km to 1 mm hr^{-1} for the ranges > 100 km. The distribution of land/TD is broader than that of ocean/TD in the inner 100 km, and vice versa in the region beyond 100 km. The mode of the land/TS (ocean/TS) distribution as showed in Fig. 4c (Fig. 4d) decreases from 2.5 (2.5) mm hr^{-1} in the inner 100 km to 1.5 (0.9) mm hr^{-1} for the ranges > 100 km. It is interesting to note that in the inner 200 km, the land/TS contains a higher percentage of rain rates > 10 mm hr^{-1} than ocean/TS. This high end could explain why even some tropical storms could produce catastrophic inland flooding such as Tropical Storm Allison (2001). Generally, the distribution of land/HUR (Fig. 4e) is broader than that of ocean/HUR (Fig. 4f) for all radii, indicating a more asymmetric feature for hurricanes over land than over ocean. Multiple modes are found for the land/HUR 2D frequency distribution for all radii with the maximum rain rate of 10.5 mm hr^{-1} in the inner 50 km, 4 mm hr^{-1} at 350-km radius, and around 0.5 mm hr^{-1} at 1000-km radius. The mode of ocean/HUR has a smooth

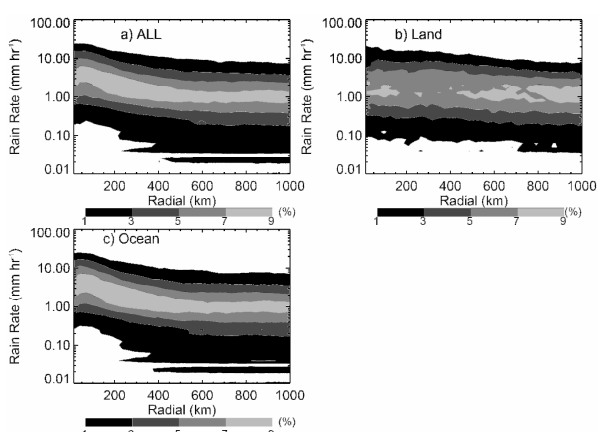

Figure 3. Radial distribution of rainfall PDFs computed for a) all 2680 observations, b) over-land observations, and c) over-ocean observations. The color scale refers to the frequency of occurrence of rain rates at any radial distance from the storm center.

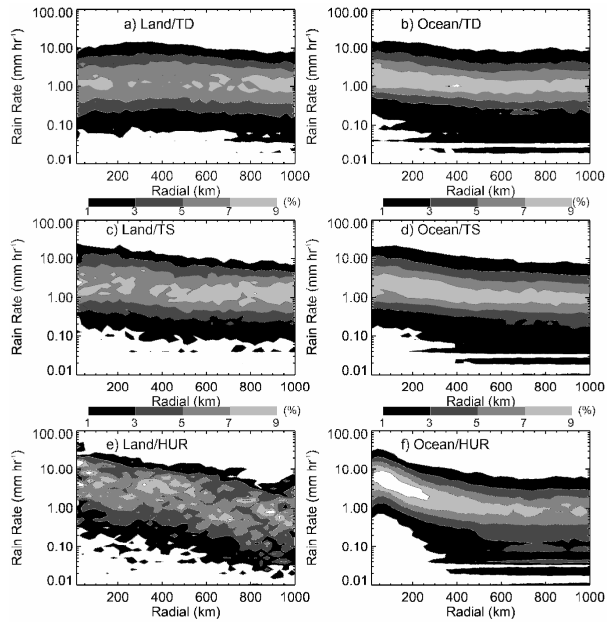

Figure 4. Radial distribution of rainfall PDFs computed for a) over-land/TD, b) over-ocean/TD, c) over-land/TS, d) over-ocean/TS, e) over-land/HUR, and f) over-ocean/HUR observations. The color scale refers to the frequency of occurrence of rain rates at any radial distance from the storm center.

decreasing from 7-8 mm hr^{-1} in the inner 100 km to about 1 mm hr^{-1} by the 400-km radius. The peak remains at 1 mm hr^{-1} at ranges > 400 km.

d. Correlations with Maximum Wind Intensity

Fig. 5 demonstrates the correlations between mean rain rate as a function of radial distance and TC

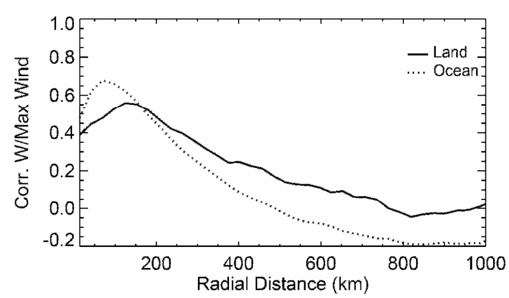

Figure 5. Correlations between mean rain rate as a function of radial distance and TC maximum wind intensity for over-land and over-ocean observations.

maximum wind intensity for over-land and over-ocean observations. Table 3 lists these correlations for upto 3° radius. The highest correlation for the over-ocean observations is 0.68 at the about 80-km radius. The highest correlation for the over-land observations is 0.55 at the about 120-km radius. It is obvious that in the inner

Table 3: Linear correlation coefficient between mean rain rate as a function of radial distance and TC maximum wind intensity for over-land and over-ocean observations.

Radius (°)	0° - 0.25°	0.25° - 0.5°	0.5° - 0.75°	0.75° - 1°	1° - 1.25°	1.25° - 1.5°	1.5° - 1.75°	1.75° - 2°	2° - 2.25°	2.25° - 2.5°	2.5° - 2.75°	2.75° - 3°
Radial Distance (km)	14	42	70	98	125	153	181	208	236	264	292	319
Coefficients for over land	0.39	0.45	0.48	0.53	0.56	0.55	0.52	0.47	0.42	0.40	0.36	0.32
Coefficients for over ocean	0.48	0.62	0.68	0.66	0.62	0.57	0.49	0.43	0.37	0.31	0.26	0.21

150 km where the rain rate is highly correlated with the storm intensity, rains over land has a much weaker relationship with the storm maximum wind intensity than rains over ocean. From Fig. 5, we can also see that at ranges > 150 km from the TC center, the correlations for over-land rains are higher than those for over-ocean rains, but the values of correlations are generally so low that they will not be discussed.

Many studies (Rodgers et al. 1995, Rodgers and Pierce 1994, Rodgers et al. 2001) have shown that the inner-core (within 111-km radius) mean rain rate is a good indicator of storm intensity, because the inner core latent heating release that is directly related to the inner core mean rain represents the major energy source for TC intensification. Fig. 6 displays the storm maximum wind intensity as a function of inner core mean rain rates for over-land and over-ocean groups, respectivelyIn general, more intense TCs over land are associated with higher inner core mean rain rate, but the overall correlation is only 0.51 and there is a large amount of scatter in the relationship (Fig. 6a). In the over-ocean scatter plot (Fig. 6b), although there are still many outliers, the correlation reaches 0.7, indicating that when TCs are over ocean, the inner core mean rain rate is well correlated with TC intensity. But when TCs are over land, the correlation is much weaker.

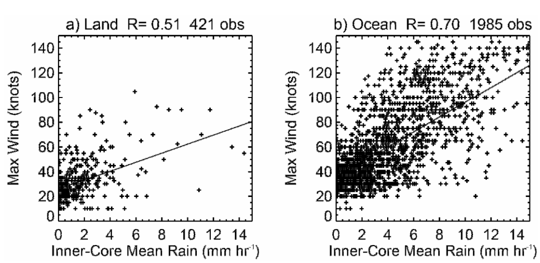

Figure 6. Maximum wind intensity at the time of the MPA estimates as a function of inner core (0°-1° radius) mean rain rate for a) over-land and b) over-ocean observations.

4. RELATIONSHIPS BETWEEN RAIN POTENTIAL AND TC LANDFALL RAIN

One of the main questions in this study asks whether the rainfall potential when the storm over ocean could be used a good predictor of the storm's potential on inland flooding. To test this, the relationships between a set of rainfall potential parameters for different time periods before landfall and TC landfall total rain parameters are examined using the 1998-2004 Atlantic landfall TC dataset. A prediction index for TC landfall rain is proposed and verified by using a 2005 Atlantic landfall hurricane (Katrina).

a. Relationships

Several TC landfall rain parameters are selected to examine their relationship with the rainfall potential. These parameters consists of the maximum storm total rain during US land-rain period (mm), mean daily rain over land (mm day^{-1}), mean daily volumetric rain over land (km^3 day^{-1}), storm total volumetric rain on the landfall day (km^3 day^{-1}), storm total volumetric rain for 0-1 day after landfall (km^3 day^{-1}), storm total volumetric rain for 0-2 day after landfall (km^3 day^{-1}). Among these parameters, only the maximum storm total rain during US land-rain period is obtained from surface rain gauge measurements, all others are derived from the satellite-based MPA product. The rain gauge-based maximum storm total rain is our main parameter as the indicator of the TC inland flooding, while all the satellite-based parameters could be as an additional set of parameters to demonstrate the TC landfall total rain. Fig. 7 shows the correlations between these parameters and the rainfall potential for 0-4 days before TC landfall for all 37 TCs that made landfall in the US Gulf coast during 1998-2004 (see table 1), sub-samples that made landfall at hurricane stage (HUR, 13 storms), and those that made landfall at tropical storm stage (TS, 24 storms). These correlations are calculated in logarithm scale. Table 4 lists these correlations. Fig. 7 clearly implies that the rainfall potential is highly correlated with the maximum storm total rain during US land-rain period. Comparing Fig. 7a-c, it is apparent that the highest of these correlations (0.78) emerges from the maximum storm total rain of the HUR sample with the rain potential for 1 day before landfall. All satellite-based TC landfall rain parameters produce lower correlations

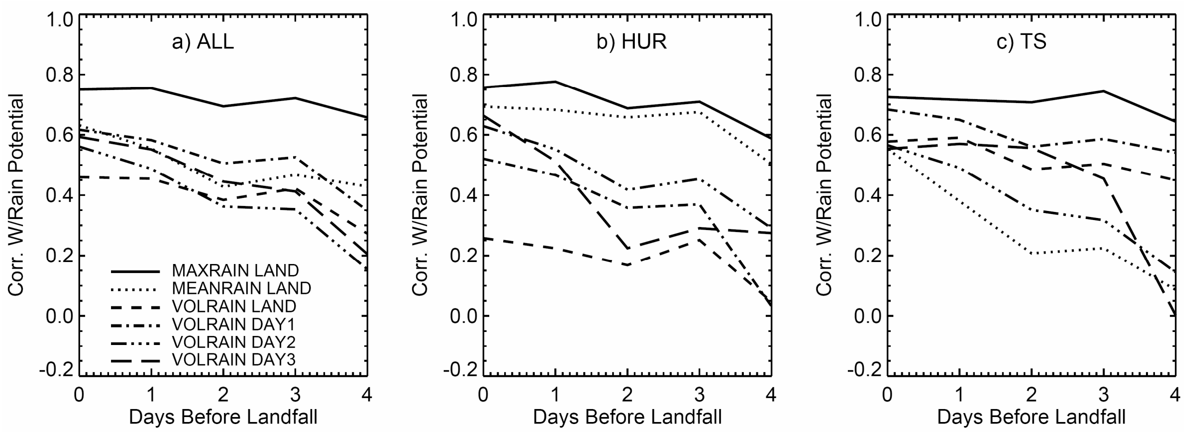

Figure 7. Correlations between TC landfall rain parameters including the maximum storm total rain during landfall (MAXRAIN LAND, mm), mean daily rain over land (MEANRAIN LAND, mm day^{-1}), mean daily volumetric rain over land (VOLRAIN LAND, km^3 day^{-1}), storm total volumetric rain on the landfall day (VOLRAIN DAY1, km^3 day^{-1}), storm total volumetric rain for 0-1 day after landfall (VOLRAIN DAY2, km^3 day^{-1}), storm total volumetric rain for 0-2 day after landfall (VOLRAIN DAY3, km^3 day^{-1}) and rainfall potential for 0-4 days before landfall for a) All, b) HUR only, and c) TS only. HUR and TS represent the storm stage during landfall. TC landfall rain parameters and rainfall potentials are in log scale.

Table 4: Linear correlation coefficient between TC landfall rain parameters and rainfall potential for 0-4 days before landfall in the log scale for all samples (All), TCs with landfall intensity stage as hurricane (HUR), and TCs with landfall intensity stage as tropical storm (TS).

	All Samples (HUR) [TS]					
	Maximum Storm Total Rain During Landfall	Mean Daily Rain Over Land	Mean Daily Volumetric Rain Over Land	Storm Total Volumetric Rain on the Landfall Day	Mean Storm Total Volumetric Rain on 0-1 Days After Landfall	Mean Storm Total Volumetric Rain on 0-2 Days After Landfall
Rain Potential on the Landfall Day	0.75 (0.76) [0.72]	0.63 (0.69) [0.55]	0.46 (0.26) [0.58]	0.62 (0.52) [0.68]	0.56 (0.63) [0.57]	0.59 (0.66) [0.55]
Rain Potential for 1 day before Landfall	0.75 (0.78) [0.72]	0.55 (0.68) [0.38]	0.45 (0.22) [0.59]	0.58 (0.47) [0.65]	0.49 (0.55) [0.49]	0.55 (0.51) [0.57]
Rain Potential for 2 day before Landfall	0.69 (0.69) [0.71]	0.43 (0.66) [0.21]	0.38 (0.17) [0.49]	0.51 (0.36) [0.56]	0.36 (0.42) [0.35]	0.44 (0.22) [0.56]
Rain Potential for 3 day before Landfall	0.72 (0.71) [0.74]	0.47 (0.68) [0.22]	0.42 (0.25) [0.50]	0.53 (0.37) [0.59]	0.35 (0.45) [0.32]	0.41 (0.29) [0.45]
Rain Potential for 4 day before Landfall	0.66 (0.59) [0.64]	0.43 (0.50) [0.09]	0.27 (0.05) [0.45]	0.35 (0.03) [0.54]	0.15 (0.29) [0.14]	0.21 (0.27) [0.00]

with the rainfall potential before landfall for the ALL, HUR, and TS samples, expect that the mean daily rain over land for the HUR sample produces comparable correlations with the rain potentials as the maximum storm total rain parameter.

More insight into the relationships between TC landfall rain and rainfall potential can be found by examining scatterplots of the data. Fig. 8 presents scatter plots and linear correlations between, landfall hurricanes (Fig. 8b), and landfall tropical storms (Fig. 8c). From Fig. 8, in general, more intense TC inland flooding is associated with high rainfall potential before TC's landfall. The correlations are 0.75, 0.78, and 0.72 for ALL, HUR, and TS sample, respectively. Significant tests for these correlations show that confidence levels are above 99%. However, there is a certain amount of scatters in the relationships. The greatest outlier is hurricane Georges (1998). This might be associated with the TC landfall complicated factors such as topography and trough interactions.

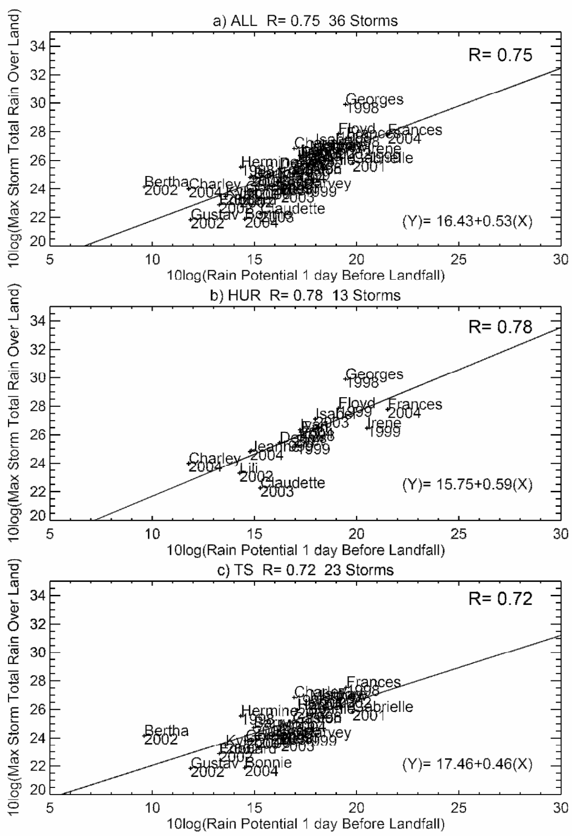

Figure 8. Scatter plots and linear correlations between the maximum storm total rain during US land-rain period (mm) and rain potential for 1 day before landfall in log scale for a) all landfall tropical cyclones; b) for landfall hurricanes; c) for landfall tropical storms. Storm names and years are indicated. The correlation coefficients and linear fit equations are also indicated.

b. A prediction index for TC landfall rain

According to the logarithm-scale linear fitting equation between the maximum storm total rain and rain potential for 1 day before landfall for all landfall TCs (Fig. 8a), we have:

$$MaxRain = 44RP^{0.53} \quad (3)$$

where *MaxRain* is the maximum storm total rain over land in mm, *RP* is rain potential for 1 day before landfall. This relationship is plotted in Fig. 9. A prediction index for TC landfall rain is proposed and given in table 5 according to Fig. 9. This index is to use the rainfall potential for 1 day before landfall derived from the satellite-based MPA product to predict the maximum storm total rain over land. Five categories of TC landfall rain intensity are set up according to this index. As the index increases from 1 to 5, the predicted TC maximum storm total rain over land increases from less than 6 in (149 mm) to greater than 20 in (505 mm).

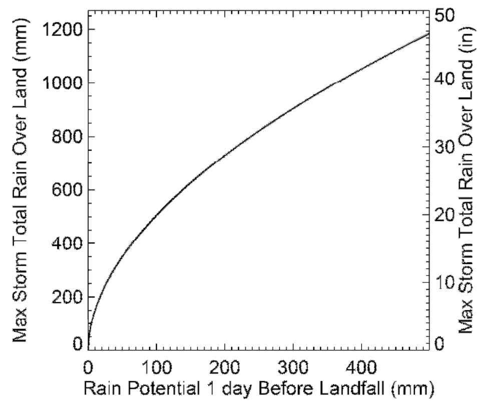

Figure 9. Relationship between the maximum storm total rain over land and rainfall potential 1 day before landfall.

Table 5: TC landfall rain prediction index. Maximum storm total rain over land is shown in both mm and in.

Index	Rainfall potential for 1 day before landfall (mm)	Maximum storm total rain over land	
		(mm)	(in)
1	<10	<149	<6
2	10 ~ 30	149 ~ 267	6 ~ 10
3	30~ 60	267 ~ 385	10 ~ 15
4	60 ~ 100	385 ~ 505	15 ~ 20
5	>= 100	>= 505	>= 20

To verify this prediction index, hurricane Katrina (23-31 August 2005) case is presented below. Katrina was the 12th Atlantic TC of 2005. It was extraordinary powerful and deadly, and was the costliest and one of the five deadliest hurricanes to ever strike the United States. Katrina formed from the interaction of a tropical wave, the middle tropospheric remnants of Tropical Depression Ten, and an upper tropospheric trough over the southeastern Bahamas on 23 August and moved westward. The "best track" of the path of the center Katrina is displayed in Fig. 10. It intensified to tropical storm stage on 24 August and hurricane status on 25 August, right before its center made landfall on the southeastern coast of Florida. After weakening to tropical storm over land, Katrina was back to water of Gulf of Mexico and quickly regained hurricane status at 26 August. Then rapid intensification occurred during 26-28 August and Katrina attained its peak intensity of 150 kt (category 5 in Saffir-Simpson Hurricane Scale) at 1800 UTC 28 August at southeast of the mouth of the Mississippi River. Rapid weakening was observed prior to Katrina’s final landfall. Katrina made landfall at the Louisiana/Mississippi border as a category 3 hurricane on 29 August. Once it moved inland, Katrina weakened to a tropical depression and moved northeastward across the southeastern United States. The maximum storm total rain caused by Katrina’s first landfall in the United States was 16.43 inches reported by the station at Perrine, FL. For Katrina’s second landfall, the maximum storm total rain was 14.82 inches reported at the Big Branch, LA.

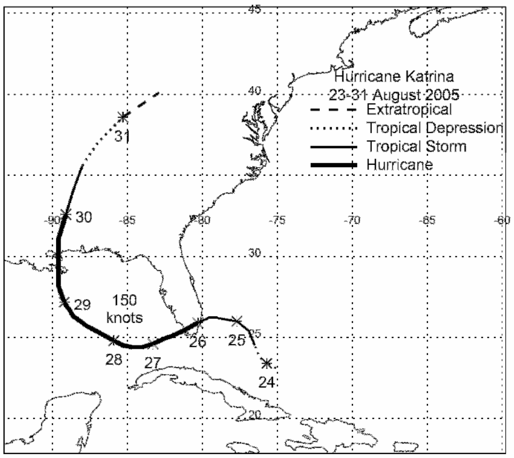

Figure 10. Best-track location and intensity (see legend) for North Atlantic hurricane Katrina (23-31 August 2005). The maximum wind speed intensity on 28 August is indicated.

Fig. 11 shows MPA derived daily rain accumulations for hurricane Katrina between 23 and 31 August, 2005. Using the MPA data, rainfall potentials for Katrina are calculated using (1). Table 6 gives rainfall potentials for 1 day before Katrina’s first and second landfall in the United States. Predicted and observed maximum storm total rains over land and the prediction errors for these two landfall periods are also presented. By using the TC landfall rain prediction index, Katrina’s first (second) landfall is predicted to be in category 4 (3) of the landfall rain intensity with the predicted maximum storm total rain over land of 17.71 (14.54) inches. Comparing with the observed values, the error of this prediction is within 10%.

5. SUMMARY

Rainfall distributions over land and ocean in Atlantic TCs have been studied using observations from MPA. Between 1 January 1998 and 31 December 2004, 2680 3-hourly instantaneous MPA measurements were collected in 37 Atlantic landfall TCs with intensity ranging from tropical depression to category 5 hurricane. PDFs and azimuthal averages are constructed as a function of TC intensity and location. Correlations between rain rate and maximum wind intensity for over-land and over-ocean observations are compared.

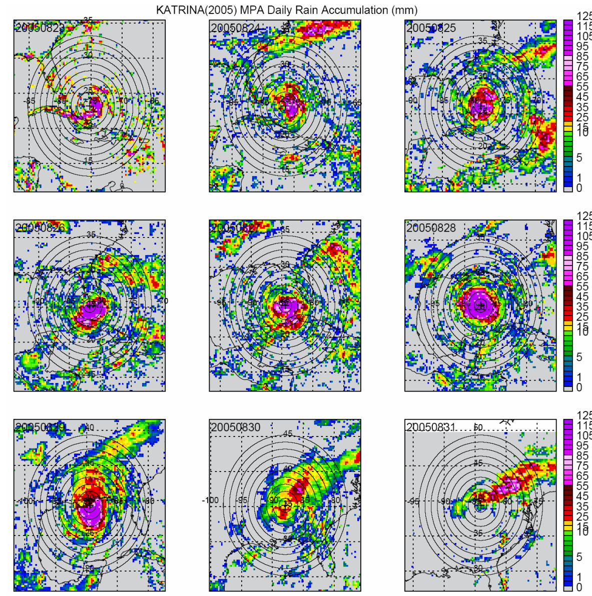

Figure 11. MPA derived daily rain accumulations (mm) for hurricane Katrina between 23 and 31 August, 2005.

Table 6: Hurricane Katrina (2005)’s rainfall potential derived from the satellite based MPA product for 1 day before Katrina’s first and second landfall. Predicted and observed maximum storm total rains over land and the prediction errors for these two landfall periods are also shown.

Landfall Date (mmdd)	Rainfall Potential (mm)	Maximum Storm Total Rain (in)		Error
		Predicted	Observed	
0826	80.45	17.72	16.43	7.8%
0829	55.40	14.45	14.82	1.8%

The PDF and azimuthal average analysis is used for comparison of MPA TC rainfall distributions with previous studies and for comparison of over-land and over-ocean differences. It is found that over-ocean distributions derived from the MPA product have the similar characteristics to those results in previous studies (Rodger et al. 1994, Rodger and Pierce 1995, Lonfat et al. 2004). However, peak value and location of peak for over-land distributions are significantly different with those for over-ocean distributions, indicating stronger rains for over-land observations. Many previous studies (Rodger et al. 1995, Rodger and Pierce 1995, Rodger et al. 2001) have shown that the inner-core mean rain is well correlated with TC intensity. However, this study found that this statement might be only true for over-ocean observations. For TCs over land, the correlation is much weaker.

Using the same dataset, the relationships between rainfall potential and TC landfall rain parameters have been examined. High correlations are found between rainfall potential for 1 day before TC landfall and maximum storm total rain over land. A prediction index is proposed based this finding. Hurricane Katrina (2005) case is applied to verify this prediction index. By comparing with surface rain gauge observations, the error of the forecasted TC landfall rain is within 10%. Future work is to verify this index using more 2005 hurricane cases.

ACKNOWLEDGEMENTS

The authors would like to thank Drs. Edward J. Zipser and Scott Braun for providing support and valuable comments on this study. Thanks to Drs. Robert Adler and George Huffman for providing MPA-RT data. Thanks to Drs. David Roth, and James Franklin for their assistance on TC surface rainfall and best track data. Thanks are given to Manuel Lonfat for discussion and feedback. This research was supported by the NASA PMM grant. The authors would like to thank Ramesh Kakar (NASA headquarters) for his continued support of PMM science.

REFERENCES

Adler, R.F., G. J. Huffman, A. Chang, R. Ferraro, P. Xie, J. Janowiak, B. Rudolf, U. Schneider, S. Curtis, D. Bolvin, A. Gruber, J. Susskind, and P. Arkin, 2003: The Version 2 Global Precipitation Climatology Project (GPCP) Monthly Precipitation Analysis (1979-Present). *J. Hydrometeor.*, **4**, 1147-1167.

____, G. J. Huffman, P.R. Keehn, 1994: Global Tropical Rain Estimates from Microwave-Adjusted Geosynchronous IR Data. *Remote Sensing Rev.*, **11**, 125-152.

____, A. J. Negri, P. R. Keehn, and I. M. Hakkarinen, 1993: Estimation of monthly rainfall over Japan and surrounding waters from a combination of low-orbit microwave and geosynchronous IR data. *J. Appl. Meteor.,* **32**, 335-356.

Atallah, E. H., and L. F. Bosart. 2003: The extratropical transition and precipitation distribution of Hurricane Floyd (1999)**.** *Mon. Wea. Rev.*, **131**, 1063-1081.

Carr, F. H., and L. F. Bosart, 1978: A diagnostic evaluation of rainfall predictability for Tropical Storm Agnes, June 1972. *Mon. Wea. Rev.*, **106**, 363–374.

Elsberry, R. L., 2002: Predicting hurricane landfall precipitation. *Bul. Amer. Meteor. Soc.*, **83**, 1333-1340.

Elsberry, R. L., 2005: Achievement of USWRP hurricane landfall research goal. *Bul. Amer. Meteor. Soc.*, **86**, 643-645.

Griffith, C. G., W. L. Woodley, P. G. Gube, D. W. Martin, J. Stout and D. N. Sikdar, 1978: Rain estimates from geosynchronous satellite imagery: Visible and infrared studies. *Mon. Wea. Rev.*, **106**, 1153-1171.

Heymsfield, G. M., J. B. Halverson, J. Simpson, L. Tian, and T. P. Bui, 2001: ER-2 Doppler radar investigations of the eyewall of Hurricane Bonnie during the Convection and Moisture Experiment-3. *J. Appl. Meteor.,* **40**, 1310–1330.

Huffman, G. J., R.F. Adler, E. F. Stocker, D.T. Bolvin, E. J. Nelkin, 2003: Analysis of TRMM 3-hourly multi-satellite precipitation estimates computed in both real and post-real time. Proc. 12th Conf. Satellite Meteorology and Oceanography, AMS, Feb. 10-13, 2003, Long Beach, CA.

Huffman, G.J., R.F. Adler, M. Morrissey, D.T. Bolvin, S. Curtis, R. Joyce, B McGavock, J. Susskind, 2001: Global Precipitation at One-Degree Daily Resolution from Multi-Satellite Observations. *J. Hydrometeor.,* **2**, 36-50.

Jiang, H., J. B. Halverson, and J. Simpson, 2005: On the difference of storm wetness of hurricane Isidore and Lili. Part I: Satellite observations and rain potential. *Wea. Forecasting*, submitted.

Kummerow, C., W. S. Olson, and L. Giglio, 1996: A simplified scheme for obtaining precipitation and vertical hydrometeor profiles from passive microwave sensors. *IEEE Trans. Geosci. Remote Sens.*, **34**, 1213-1232.

Lonfat, M., F. D. Marks, and S. S. Chen, 2004: Precipitation distribution in tropical cyclones using the Tropical Rainfall Measuring Mission (TRMM) microwave imager: A global perspective. *Mon. Wea. Rev.*, **132**, 1645–1660.

Malkus, J., and H. Riehl, 1960: On the dynamics and energy transformations in steady-state hurricanes. *Tellus*, **12**, 1-20.

Miller, B. I., 1958: Rainfall rates in Florida hurricanes. *Mon. Wea. Rev.*, **86**, 258-264.

Rappaport, E. N., 2000: Loss of life in the United States associated with recent Atlantic tropical cyclones. *Bul. Amer. Meteor. Soc.*, **81**, 2065-2074.

Rao, G. V., and P. D. MacArthur, 1994: The SSM/I estimated rainfall amounts of tropical cyclones and their potential in predicting the cyclone intensity changes. *Mon. Wea. Rev.*, **122**, 1568-1574.

Rodgers, E. B., and R. F. Adler, 1981: Tropical cyclone rainfall characteristics as determined from a satellite passive microwave radiometer. *Mon. Wea. Rev.*, **109**, 506-521.

____, and H. F. Pierce, 1995: A satellite observational study of precipitation characteristics in western North Pacific tropical cyclones. *J. Appl. Meteor.,* **34**, 2587-2599.

____, S. W. Chang, and H. F. Pierce, 1994: A satellite observational and numerical study of precipitation characteristics in western North Atlantic tropical cyclones. *J. Appl. Meteor.,* **33**, 129-139.

Weng, F., L. Zhao, R. Ferraro, G. Poe, X. Li, and N. Grody, 2003: Advanced Microwave Sounding Unit cloud and precipitation algorithms. *Radio Sci.*, **38**, 8068–8079.

Zhao, L., and F. Weng, 2002: Retrieval of ice cloud parameters using the Advanced Microwave Sounding Unit. *J. Appl. Meteor.*, **41**, 384-395.